Mon. Not. R. Astron. Soc. **268**, 1–12 (1994)

A study of the Chamaeleon I dark cloud and T-association – VI. Interstellar polarization, grain alignment and magnetic field

D. C. B. Whittet,[1,2] P. A. Gerakines,[1,3] A. L. Carkner,[1,4] J. H. Hough,[5] P. G. Martin,[6] T. Prusti[7] and D. Kilkenny[8]

[1] *Department of Physics, Rensselaer Polytechnic Institute, Troy, NY 12180, USA*
[2] *Kapteyn Astronomical Institute and Laboratory for Space Research, PO Box 800, 9700 AV Groningen, The Netherlands*
[3] *Present address: Leiden Observatory, PO Box 9513, 2300 RA Leiden, The Netherlands*
[4] *Present address: Department of Astronomy and Astrophysics, Pennsylvania State University, University Park, PA 16802, USA*
[5] *Division of Physical Sciences, University of Hertfordshire, College Lane, Hatfield, Hertfordshire AL10 9AB*
[6] *Canadian Institute for Theoretical Astrophysics, University of Toronto, Toronto, Ontario M5S 1A1, Canada*
[7] *Astrophysics Division, Space Science Department, ESTEC, PO Box 299, 2200 AG Noordwijk, The Netherlands*
[8] *South African Astronomical Observatory, PO Box 9, Observatory, Cape 7935, South Africa*

Accepted 1993 October 12. Received 1993 October 8; in original form 1993 July 16

ABSTRACT

We present new measurements of optical and near-infrared linear polarization towards 39 field stars reddened by dust in the Chamaeleon I dark cloud. New and previously published data are combined in a detailed investigation of the wavelength dependence of interstellar polarization in the cloud. The observations are well represented by the Serkowski formula, with values of the wavelength of maximum polarization (λ_{max}) in the range 0.47–0.75 μm. The highest values of λ_{max} are found in lines of sight that intercept the dense central region of the cloud. The ratio of total to selective extinction ($R_V = A_V/E_{B-V}$) is only weakly correlated with λ_{max}, suggesting a degree of independence among the populations of grains responsible for optical extinction and polarization.

We show that the ratio of polarization to reddening is unusually high in Cha I, with $p_{max}/A_V \simeq 4.5$ per cent mag^{-1} in some lines of sight, indicating a remarkable degree of alignment efficiency in comparison to other dark clouds. The mean direction of the magnetic field in the plane of the sky is perpendicular to the long axis of the cloud and parallel to the external magnetic field in the Galactic neighbourhood of Chamaeleon, suggesting that the cloud formed by uniform collapse along field lines. Our observations provide important constraints on theoretical models for both grain alignment and the relation between magnetic field, cloud collapse and star formation.

Key words: polarization – stars: formation – ISM: clouds – dust, extinction – ISM: individual: Chamaeleon I – ISM: magnetic fields.

1 INTRODUCTION

Magnetic fields undoubtedly have a profound effect on the evolution of interstellar clouds and may control the fragmentation of clouds to form new stars (Mouschovias & Morton 1991 and references therein). One of the most readily observable phenomena arising from the presence of magnetic fields is the linear polarization of starlight, attributed to extinction by partially aligned, aspherical grains. Although the alignment mechanism is not fully understood, it is clear that the magnetic field is responsible for alignment, with the long axes of the grains tending to become orientated perpendicular to the field lines. Observations of the polarization of background stars define the morphology of the magnetic field in the plane of the sky, and provide insight into the effect of the field on the geometrical structure of a collapsing cloud (e.g. Goodman et al. 1990). They also provide an important means of investigating the optical properties of the dust grains as a function of environment.

The Chamaeleon I dark cloud is ideally suited to such a study. It contains one of the closest regions of recent star formation, situated ~ 140 pc from the Solar system. In previous papers, we have investigated the nature of the stellar population towards the cloud, distinguishing between field stars and members of the T-association, and deducing a luminosity function for the newly formed stars (Whittet et al. 1987, Paper I; Assendorp et al. 1990, Paper II; Whittet, Prusti & Wesselius 1991, Paper III; Prusti et al. 1991a, Paper IV; Prusti, Whittet & Wesselius 1992, Paper V). A number of reddened background field stars were identified in Paper I; these objects are obscured

Table 1. Three-colour (*B, I, J*) polarimetry.

Star	p_B	θ_B	p_I	θ_I	p_J	θ_J
Cha F1	3.25± 0.06	118± 1	3.23± 0.11	116± 1	1.91± 0.06	117± 1
Cha F4	3.04± 0.06	123± 1	2.47± 0.06	121± 1	1.62± 0.04	127± 1
Cha F5	2.40± 0.20	134± 1	2.30± 0.40	132± 3	1.56± 0.19	130± 3
Cha F8	0.4 ± 0.3	129± 16	< 0.2	—	0.4 ± 0.2	133± 14
Cha F10	5.3 ± 1.0	124± 3	3.86± 0.09	119± 1	2.52± 0.13	119± 2
Cha F12	0.56± 0.21	131± 16	0.38± 0.07	123± 6	0.21± 0.10	151± 14
Cha F13	< 0.13	—	< 0.17	—	< 0.15	—
Cha F14	2.81± 0.14	111± 2	2.40± 0.10	113± 1	1.41± 0.06	109± 2
Cha F15	2.38± 0.08	123± 2	2.09± 0.07	125± 1	1.37± 0.09	125± 2
Cha F17	4.16± 0.22	125± 2	3.81± 0.08	124± 1	2.16± 0.11	122± 2
Cha F18	—	—	3.76± 0.26	135± 1	2.39± 0.07	134± 1
Cha F19	—	—	3.19± 0.06	130± 1	2.38± 0.08	127± 1
Cha F20	< 0.12	—	< 0.07	—	< 0.11	—
Cha F22	6.29± 0.49	120± 2	7.09± 0.17	119± 1	4.82± 0.14	121± 1
Cha F23	6.70± 0.50	116± 2	6.90± 0.09	114± 1	4.78± 0.10	118± 1
Cha F24	3.16± 0.06	131± 1	2.66± 0.07	128± 1	1.61± 0.10	128± 2
Cha F25	8.80± 0.35	123± 1	7.58± 0.10	122± 1	4.64± 0.09	122± 1
Cha F26	2.06± 0.09	129± 2	2.07± 0.11	128± 1	1.15± 0.06	126± 2
Cha F31	< 0.21	—	< 0.09	—	< 0.09	—
Cha F33	—	—	4.45± 0.18	150± 1	2.85± 0.09	151± 1
Cha F34	9.2 ± 0.8	137± 3	8.55± 0.11	132± 1	5.31± 0.13	130± 1
Cha F35	< 0.14	—	< 0.09	—	< 0.09	—
Cha F37	3.48± 0.23	120± 2	2.89± 0.06	121± 1	1.62± 0.07	116± 1
Cha F38	2.17± 0.12	121± 2	1.98± 0.06	119± 1	1.21± 0.08	119± 2
Cha F39	3.40± 0.07	127± 1	2.72± 0.05	127± 1	1.59± 0.07	125± 2
Cha F41	2.48± 0.11	122± 2	2.52± 0.14	122± 1	1.60± 0.09	119± 2
Cha F42	2.85± 0.18	121± 1	2.66± 0.07	119± 1	1.62± 0.11	123± 2
Cha F43	2.33± 0.13	124± 1	2.11± 0.06	124± 1	1.33± 0.08	125± 2
Cha F44	< 0.18	—	0.23± 0.08	150± 8	< 0.14	—
Cha F45	< 0.06	—	< 0.13	—	< 0.20	—
Cha F46	< 0.30	—	< 0.18	—	< 0.09	—
Cha F47	< 0.15	—	< 0.10	—	< 0.12	—
Cha F48	2.30± 0.25	126± 3	1.98± 0.14	127± 1	1.24± 0.09	130± 1
Cha F49	< 0.19	—	< 0.12	—	< 0.17	—
Cha F50	1.67± 0.13	137± 2	1.34± 0.16	138± 2	0.79± 0.07	141± 4
Cha F51	< 0.16	—	< 0.10	—	< 0.12	—
Cha F52	2.96± 0.10	130± 1	2.76± 0.06	130± 1	1.77± 0.09	129± 1
Cha F53	< 0.20	—	< 0.14	—	< 0.09	—
Cha F54	2.71± 0.08	125± 1	2.47± 0.07	126± 1	1.44± 0.09	126± 2

predominantly by dust in the dark cloud itself and are thus suitable for studies of the interstellar extinction, polarization and grain alignment within the cloud. Vrba & Rydgren (1984) previously investigated interstellar extinction in the visible to near-infrared towards several stars in this list, and found evidence for spatial variations characterized by changes in the ratio of total to selective extinction ($R_V = A_V/E_{B-V}$). Values of $R_V \simeq 5$ are found in the dense central regions of the cloud such as that containing the embedded zero-age main-sequence (ZAMS) star HD 97300, compared with the normal value of 3.1 in the diffuse interstellar medium (see Schwartz 1991 for further discussion and references). Such a difference in the optical properties of the grains is likely to reflect physical processes occurring within the dark cloud environment, such as grain growth by mantle condensation or grain–grain coagulation. These processes may also affect the polarizing properties of aligned grains, influencing the wavelength dependence of polarization and the efficiency with which the particles are aligned by the ambient magnetic field.

In this paper, we present observations of optical and near-infrared linear interstellar polarization towards 39 stars listed in the field star catalogue (Paper I). The observations are described in Section 2. New and previously published data are combined in a detailed investigation of the wavelength dependence of polarization (Section 3) and the magnetic field geometry and alignment efficiency of the cloud (Section 4). Our conclusions are summarized in Section 5. Finally, data presented here and elsewhere have led to a revision of the membership status of two individual stars discussed in Appendix A.

2 OBSERVATIONS

Programme stars were selected from 54 field stars catalogued in Paper I. Multiwaveband polarimetry for 15 of these has previously been reported by Whittet et al. (1992). The main aim of the observing programme reported here was to obtain measurements of polarization towards the remaining 39 stars (Section 2.1). In order to compare extinction and polarization properties, we also require photometry in optical and near-infrared passbands. This is available in the existing literature for the majority of our programme stars, but some photometric

Table 2. *UBVRI* photometry.

Star	$U-B$	$B-V$	V	$V-R$	$V-I$
Cha F4	−0.28	0.13	6.67	0.10	0.20
Cha F5	−0.24	0.18	9.00	0.14	0.29
Cha F8	0.01	0.48	8.79	0.28	0.55
Cha F12	0.07	0.14	7.33	0.08	0.16
Cha F14	−0.20	0.22	8.69	0.15	0.32
Cha F15	−0.14	0.12	7.98	0.08	0.17
Cha F26	0.23	0.28	10.13	0.18	0.38
Cha F38	0.25	0.33	7.66	0.19	0.39
Cha F44	−0.12	−0.01	6.25	−0.02	−0.03
Cha F47	0.10	0.19	6.43	0.10	0.20
Cha F51	0.08	0.59	9.37	0.31	0.63
Cha F54	0.78	1.15	8.37	0.62	1.23

Table 3. *JHK* photometry.

Star	$J-H$	$H-K$	K
Cha F5	0.08	0.04	8.68
Cha F14	0.07	0.04	8.00
Cha F15	0.03	0.03	7.62
Cha F26	0.10	0.07	9.24
Cha F38	0.15	0.07	6.73
Cha F48	0.04	0.03	8.44
Cha F50	0.17	0.06	8.37

observations were necessary to give complete coverage: these are reported in Section 2.2.

2.1 Polarimetry

The observations were made during the course of two observing runs in 1986 May and 1987 February, with the Hatfield polarimeter on the 3.9-m Anglo-Australian Telescope (AAT) at Siding Spring Observatory, New South Wales, Australia. The construction and operation of the polarimeter are described by Brindle et al. (1986). Simultaneous observations were possible in three passbands through blue, red and infrared channels. Multipassband (*UBVRIJHK*) observations of selected stars are described elsewhere (Whittet et al. 1992). In order to obtain efficient coverage of the remaining objects in the field star catalogue, additional observations were made in three filters only, selected to be B, I and J (effective wavelengths 0.43, 0.78 and 1.21 μm). Unpolarized standard stars were also observed to check the instrumental polarization, which was found to be less than 0.03 per cent in all passbands. The polarization efficiency of the instrument was measured by the introduction of a Glan prism: this was found to be essentially 100 per cent in B and I; a small correction was applied at J. Position angles θ_λ were calibrated by observations of interstellar polarization standards, selected from Serkowski, Mathewson & Ford (1975). Our data have also been corrected for noise biasing using the analytical formula $p = p'[1-(\sigma/p')^2]^{1/2}$ (Wardle & Kronberg 1974; Clarke & Stewart 1986), where σ is the standard deviation of the observed polarization p'. Because in general $\sigma \ll p'$ for our observations, the resulting corrections are small.

The results of our polarimetric observations (p_λ and θ_λ) are given in Table 1 for each filter. The errors quoted are based on standard errors in the Stokes parameters, calculated from many individual integrations.

2.2 Photometry

Optical (*UBVRI*) photometry was obtained for 12 programme stars in 1987 April, using the St Andrews photometer on the 1.0-m telescope at the Sutherland site of the South African Astronomical Observatory. Results, listed in Table 2, are tied to the Cousins E-region photometric system as defined by Menzies, Banfield & Laing (1980). This system is not significantly different from that defined by the most recent compilation of E-region standards (Menzies et al. 1989).

Near-infrared (*JHK*) photometry was obtained for seven programme stars in 1992 May, using a nitrogen-cooled InSb photometer on the 2.2-m telescope at the La Silla site of the European Southern Observatory (ESO), Chile. An aperture of 12 arcsec and a beam throw of 19 arcsec (E–W) were used. Results were calibrated to the ESO system using standard stars from Bouchet, Manfroid & Schmider (1991), and are listed in Table 3.

3 GRAIN SIZE EFFECTS

3.1 Wavelength dependence of polarization

It is well known that the wavelength dependence of linear polarization can be described by the normalized empirical relationship

$$p_\lambda/p_{\max} = \exp[-K \ln^2(\lambda_{\max}/\lambda)], \quad (1)$$

known as the Serkowski Law, where $p_{\max}$ is the peak percentage polarization, and $\lambda_{\max}$ the wavelength corresponding to $p_{\max}$ (see Whittet 1992 and references therein). This formulation was originally proposed to describe optical data, with the width parameter K assumed to be constant at 1.15 for $\lambda_{\max}$ values typically in the range 0.3–0.8 μm (Serkowski et al. 1975). Observations in the near-infrared have led to the adoption of a modified form (Wilking et al. 1980; Wilking, Lebofsky & Rieke 1982; Whittet et al. 1992), in which K is allowed to vary. With K treated as a free parameter, least-squares fits of equation (1) to data for stars with a range of $\lambda_{\max}$ show that K and $\lambda_{\max}$ are linearly related:

$$K = c_1\lambda_{\max} + c_2, \quad (2)$$

where the current best values for the slope and intercept are $c_1 = 1.66 \pm 0.09$ and $c_2 = 0.01 \pm 0.05$ (Whittet et al. 1992). The dependence of K on $\lambda_{\max}$ reflects a systematic decrease in the width of the polarization curve with increasing $\lambda_{\max}$, known

Table 4. Values of p_{max}, λ_{max} and K from three-parameter fits. Data references (right hand column) are: 1. Whittet et al. (1992); 2. This paper, Table 1; 3. McGregor et al. (1994).

Star	p_{max}	λ_{max}	K	Data ref.
Cha F2	3.85± 0.02	0.62± 0.01	1.06± 0.04	1
Cha F3	5.40± 0.07	0.64± 0.01	1.14± 0.05	1
Cha F6	5.47± 0.04	0.57± 0.01	1.01± 0.05	1
Cha F7	5.97± 0.04	0.55± 0.01	0.94± 0.02	1
Cha F9	4.84± 0.04	0.63± 0.01	0.99± 0.03	1
Cha F11	4.82± 0.08	0.53± 0.02	0.96± 0.10	1
Cha F16	7.24± 0.08	0.62± 0.01	1.09± 0.06	1
Cha F19	3.32± 0.23	0.69± 0.15	1.17± 0.62	2, 3
Cha F21	5.41± 0.14	0.47± 0.03	0.76± 0.08	1
Cha F27	6.13± 0.18	0.58± 0.04	1.09± 0.15	1
Cha F28	7.18± 0.15	0.66± 0.03	1.00± 0.09	1, 3
Cha F29	5.05± 0.08	0.64± 0.03	0.97± 0.13	1
Cha F30	4.46± 0.05	0.57± 0.01	0.88± 0.04	1
Cha F32	2.34± 0.02	0.56± 0.01	0.87± 0.05	1
Cha F33	4.36± 0.14	0.74± 0.04	1.75± 0.27	2, 3
Cha F36	12.21± 0.20	0.64± 0.02	1.02± 0.07	1, 3
Cha F40	8.02± 0.07	0.57± 0.01	0.99± 0.06	1
Cha T21	3.10± 0.08	0.67± 0.03	1.15± 0.12	1, 3
Cha T26	3.97± 0.14	0.58± 0.05	1.05± 0.18	3
Cha T32	2.77± 0.10	0.60± 0.03	1.50± 0.18	1, 3
Cha T41	3.14± 0.07	0.70± 0.02	1.24± 0.14	1, 3
Cha W58–3	9.16± 0.33	0.62± 0.07	1.13± 0.29	3

as the Wilking law; this provides a consistent representation of systematic changes occurring within individual regions with rather different environments.

We have derived fits based on the Serkowski formula to stars in Cha I with reliable polarimetric data in several passbands. Our data are from three sources: multiwaveband data for 18 stars (15 F stars and 3 T stars) from Whittet et al. (1992); three-colour data for 25 F stars from this paper (Table 1); and additional data for 17 stars from McGregor et al. (1994). All data were obtained with the Hatfield Polarimeter on the AAT and it seems justified to combine them. Fits were carried out in the manner described by Whittet et al. (1992). For 22 stars with good spectral coverage (i.e., with data in four or more passbands), fits were carried out using equation (1) with three free parameters (p_{max}, λ_{max} and K). The resulting values of these parameters derived from the fits are listed in Table 4, and examples of fits to selected stars spanning a range in λ_{max} are shown in Fig. 1. Fig. 2 shows the correlation of λ_{max} with K for 20 stars in Table 4 (F19 and T32 are omitted due to large errors and inconsistencies between polarization measurements from different data sets; the near-infrared polarization of T32 = HD 97048 appears to be variable). The straight line (equation 2) that best fits the data in Fig. 2 has parameters $c_1 = 1.78 \pm 0.34$, $c_2 = -0.06 \pm 0.20$, consistent with those deduced for the larger sample of stars in diverse regions studied by Whittet et al. (1992).

In view of this consistency in the behaviour of K, we felt justified in attempting to enlarge our data set on p_{max} and λ_{max} by carrying out fits to those stars with measurements in three passbands only. Fits were obtained with p_{max} and λ_{max} treated as free parameters and K constrained by equation (2), using values of c_1 and c_2 (above) from Whittet et al. (1992). The resulting values of p_{max} and λ_{max} are listed in Table 5. As a test of the validity of this technique, we applied it to the stars in Table 4 *using only data in the B, I and J passbands.* The values of p_{max} and λ_{max} deduced were consistent with those listed in Table 4 to within formal errors. We are thus confident that the data from Tables 4 and 5 are homogeneous, and they have therefore been combined for the purposes of the analysis presented in the following sections.

3.2 Correlation of λ_{max} with R_V

The parameters λ_{max} and R_V are related to the mean size of the particles responsible for polarization and extinction, respectively, at visible wavelengths. In the case of polarization, Mie theory computations for idealized particles such as dielectric cylinders demonstrate that they polarize most efficiently when the quantity $2\pi a(n-1)/\lambda$ is close to unity, where a and n are the radius and refractive index of the cylinder, and thus $\lambda_{max} \simeq 2\pi a(n-1)$. In practice, the range of grain sizes that contribute to the polarization might be restricted by the alignment mechanism (Mathis 1986). If the grains that produce optical polarization contribute significantly to the optical extinction, or if they respond to environmental influences in the same way, a correlation should be expected between λ_{max} and R_V. Previous investigators have shown such a correlation to exist for data sets that combine stars with diffuse and dark-cloud extinctions (Serkowski et al. 1975; Whittet & van Breda 1978; Clayton & Mathis 1988). In this section, we extend these studies to Cha I.

In order to avoid ambiguity between effects produced by circumstellar dust and interstellar dust in the line of sight to a given star, it is important to exclude stars that have infrared excess emission arising in a circumstellar shell or disc (e.g. Whittet & van Breda 1978). This may be achieved with reference to the $J-H$, $H-K$ colour-colour diagram (e.g. Paper I). Fig. 3 shows this diagram for all stars in Cha I for which we have significant polarization data (Tables 4 and 5) and photometry available from this paper and the literature

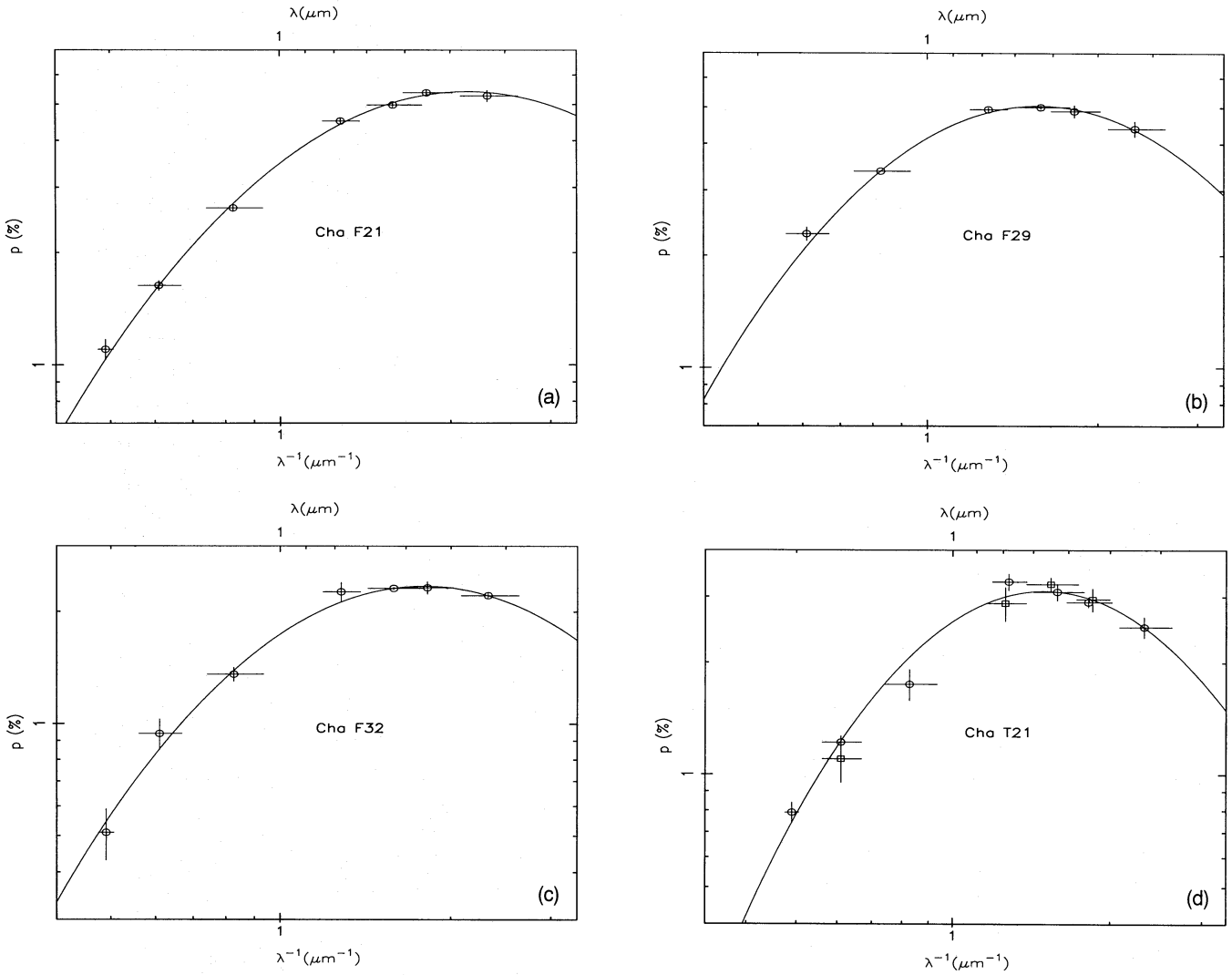

Figure 1. Sample plots of $p(\lambda)$ against λ^{-1} (points) and empirical fits (curves) based on the Serkowski formula (equation 1 and Table 4): (a) F21 (low λ_{max}); (b) F29 (intermediate λ_{max}); (c) F32 (intermediate λ_{max}); (d) T21 (high λ_{max}).

(see the footnote to Table 6 for references). Field stars and T-association members are plotted as filled circles and open circles, respectively. The solid curves represent intrinsic colour curves for dwarfs (luminosity class V) and giants (class III) from Bessell & Brett (1988), and the dotted line represents the reddening vector for average interstellar extinction (Whittet 1992) constrained to pass through the origin. As expected, Fig. 3 separates field (F) and member (T) stars (but see Appendix A for further discussion of F29 and F34, which are, in fact, probable members). Without exception, the field stars lie on or to the left of the reddening line and can be dereddened on to the intrinsic colour curves; we deduce that none of them has evidence for infrared excess at these wavelengths. In contrast, the T-stars generally lie to the right of the line. The most obvious exception is T21, which appears to be a *naked* T Tauri star without significant near-infrared excess (Paper IV). T41 (HD 97300) lies very close to the reddening line and appears to be a ZAMS B9 star with an anomalous extinction law but with otherwise normal near-infrared colours (Paper I). On the basis of Fig. 3, we include T21 and T41 with the field stars in our analysis of the λ_{max} versus R_V correlation, but exclude all other T-stars on the basis of evident infrared excess emission at 2.2 μm. The rejected stars are T26, T28, T31, T32, T33 and T44.

We deduced optical and infrared colour excesses (E_{B-V} and E_{V-K}) using intrinsic colours from Johnson (1966) and Bessell & Brett (1988) and spectral types from the literature. All results are given in Table 6, along with references to the sources of both spectral type and photometric information. Values for R_V were derived from the ratio of these colour excesses according to the relation

$$R_V \simeq 1.1 \frac{E_{V-K}}{E_{B-V}} \qquad (3)$$

based on theoretical extinction curves (e.g. Whittet & van Breda 1978), and these results are also listed in Table 6. Errors in R_V arise primarily due to uncertainties in intrinsic colours, and are typically ~ 0.2. A few cases where the error in R_V may be as high as 0.5 are identified by colons in Table 6. We did not attempt to evaluate R_V for stars with the lowest reddening ($E_{B-V} < 0.14$). There are a total of 38 stars that have both R_V

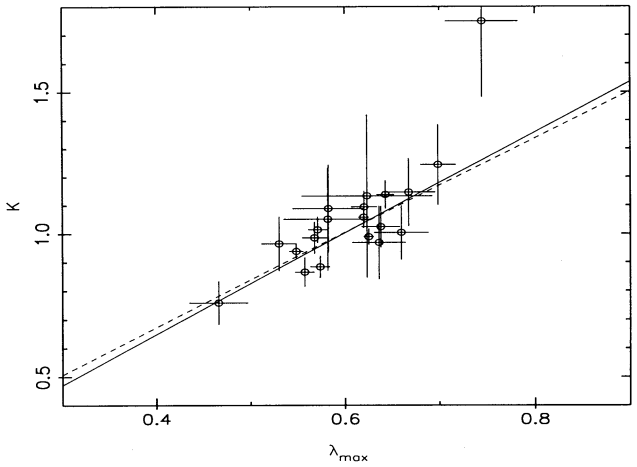

Figure 2. Plot of K against λ_{max} for 20 stars from Table 4. (F19 and T32 are omitted due to large errors and inconsistencies between polarization measurements from different data sets). The solid line is the weighted least squares best fit to the points, allowing for errors in both coordinates, and the dashed line is the best general correlation found by Whittet et al. (1992).

Table 5. Values of p_{max} and λ_{max} from two-parameter (Wilking law) fits. Data references (right hand column) are as in Table 4.

Star	p_{max}	λ_{max}	Data ref.
Cha F1	3.52± 0.07	0.57± 0.01	2
Cha F4	3.10± 0.28	0.51± 0.07	2
Cha F5	2.66± 0.13	0.59± 0.03	2
Cha F10	4.26± 0.84	0.59± 0.18	2
Cha F14	2.88± 0.02	0.51± 0.01	2
Cha F15	2.47± 0.14	0.53± 0.05	2
Cha F17	4.39± 0.22	0.53± 0.04	2
Cha F22	7.44± 0.31	0.65± 0.04	2
Cha F23	7.21± 0.59	0.66± 0.08	2
Cha F24	3.22± 0.05	0.50± 0.02	2
Cha F25	8.90± 0.59	0.53± 0.05	2
Cha F26	2.22± 0.14	0.55± 0.05	2
Cha F34	9.51± 0.40	0.57± 0.03	2
Cha F37	3.56± 0.16	0.48± 0.03	2
Cha F38	2.28± 0.04	0.54± 0.02	2
Cha F39	3.42± 0.05	0.47± 0.01	2
Cha F41	2.76± 0.03	0.59± 0.01	2
Cha F42	3.02± 0.03	0.55± 0.01	2
Cha F43	2.43± 0.11	0.54± 0.04	2
Cha F48	2.36± 0.17	0.53± 0.05	2
Cha F50	1.69± 0.04	0.48± 0.02	2
Cha F52	3.14± 0.12	0.56± 0.03	2
Cha F54	2.84± 0.03	0.53± 0.01	2
Cha T28	6.10± 0.14	0.71± 0.01	3
Cha T31	4.23± 0.14	0.75± 0.02	3
Cha T33	2.70± 0.58	0.50± 0.18	3
Cha T44	3.54± 0.41	0.46± 0.06	3
Cha C4–4	7.63± 0.15	0.70± 0.01	3
Cha C4–6	7.44± 0.18	0.71± 0.02	3
Cha C10–9	2.29± 0.30	0.65± 0.10	3
Cha W55–4	9.80± 0.45	0.71± 0.03	3

values (listed in Table 6) and λ_{max} values (listed in Table 4 or 5).

The plot of λ_{max} versus R_V for this data set is displayed in Fig. 4 (solid circles). Although there is considerable scatter, a

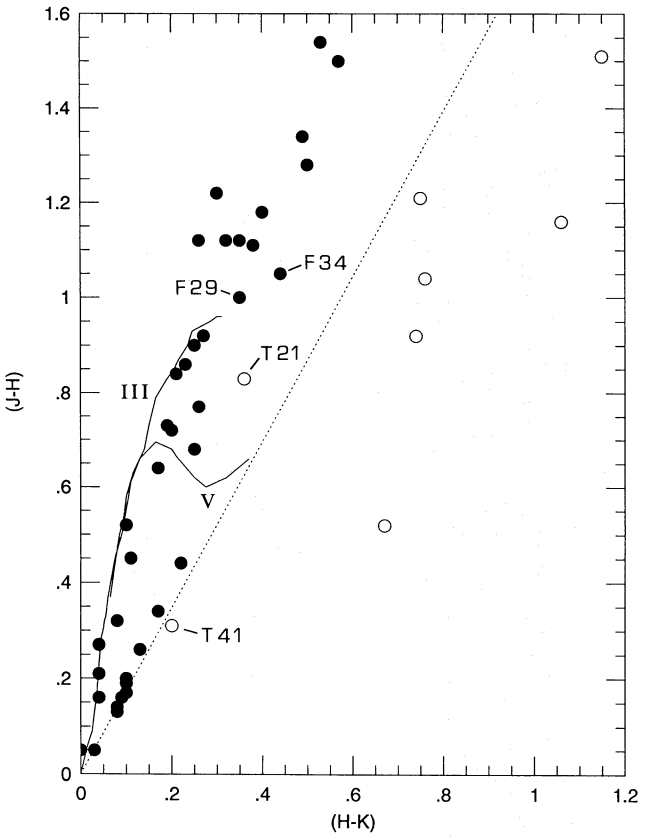

Figure 3. $J-H$, $H-K$ diagram. Filled circles represent field stars, and the open circles are T-association members, according to the classification in Paper I. The solid lines represent intrinsic colour curves for dwarf stars (luminosity class V) and giants (class III) from Bessell & Brett (1988). The dotted line represents the normal reddening vector.

clear correlation exists between the two parameters. However, this correlation differs from that found for other samples of stars (Whittet & van Breda 1978; Clayton & Mathis 1988). For illustration, we also plot in Fig. 4 data from Clayton & Mathis (hereafter CM; open circles). The CM data set contains 30 stars which sample a range of environments, including both dark clouds and diffuse regions of the interstellar medium, selected according to stringent criteria designed to eliminate all dispersion in λ_{max} and R_V due to factors other than those intrinsic to the interstellar medium. Nevertheless, in both the CM and Cha I data sets, the scatter is substantially greater than expected from observational errors. Despite considerable overlap in the distribution of points, linear least-squares fits to the two data sets yield significantly different slopes (Fig. 4). In Cha I, there is larger dispersion in R_V (in the direction of larger values) than would be expected on the basis of the dispersion in λ_{max}. Those Cha I stars that deviate most from previous correlations are characterized by polarization with rather normal λ_{max} together with extinction with rather high R_V.

3.3 Spatial distribution of grain growth

Spatial variation in the extinction curve in Cha I has been suggested by Vrba & Rydgren (1984). Fig. 5 shows the spatial distributions of (a) λ_{max} and (b) R_V on the sky from our

Table 6. Spectral types, colour excesses and R_V values (: indicates an uncertain value). In the right hand column, roman numerals refer to papers in this series (VI is the current paper: see Tables 2 and 3). Arabic numerals are as follows: 1. Vrba & Rydgren (1984); 2. Houk & Cowley (1975); 3. Glass (1979); 4. Feigelson & Kriss (1989); 5. Blanco et al. (1968); 6. Hyland, Jones & Mitchell (1982); 7. Jones et al. (1985); 8. Gregorio-Hetem et al. (1992); 9. Rydgren (1980); 10. Grasdalen et al. (1975); 11. King (1981); 12. Kilkenny et al. (1985); 13. Whittet & van Breda (1980).

Star	Sp	E_{B-V}	E_{V-K}	R_V	References
Cha F1	K4 III	0.14	0.64	5.0:	1
Cha F2	B8 V	0.58	1.75	3.32	1; III
Cha F3	B2–4 V	0.61	2.16	3.90	1,2; III
Cha F4	B8 III	0.23	0.64	3.06	2; III,VI
Cha F5	B9 V	0.22	0.46	2.3:	2; VI
Cha F6	A2 V	0.58	1.69	3.21	1
Cha F7	B5 V	0.54	1.62	3.30	1; III
Cha F8	F5 V	0.04	—	—	2; VI
Cha F9	K0 III	0.62	2.18	3.87	1
Cha F10	K3 III	0.77	2.66	3.80	3; I
Cha F11	B9 V	0.77	3.61	5.16	1
Cha F12	A2 Vn	0.09	—	—	2; VI
Cha F13	F8 V	0.02	0.04	—	2; I
Cha F15	B9 V	0.16	0.48	3.3:	2; VI
Cha F16	G2 IV	0.82	2.57	3.45	1,3; I
Cha F18	G8 III	1.27	4.83	4.18	3; I
Cha F20	K3 V	0.00	0.00	—	1; I
Cha F21	K3 III	0.64	1.89	3.25	1,3; I
Cha F22	G8 III	1.03	3.87	4.13	3; I
Cha F23	M5 III	0.88	3.13	3.91	3; I
Cha F24	B6–7 IV/V	0.28	0.99	3.89	1,2
Cha F25	G8 III	1.27	4.93	4.27	3; I
Cha F26	A1 IV	0.26	0.81	3.44	2; VI
Cha F28	K4 III	1.08	5.44	5.54	3; I
Cha F29	K7 V:	0.47:	2.49:	5.8:	1,3,4; I
Cha F30	K3 III	0.43	1.71	4.37	1,3; I
Cha F31	F5 V	0.01	0.00	—	2,3,5,6; I
Cha F32	F0 V:	0.42	1.97	5.16	1,3,7; I,V
Cha F33	G8 III	1.05	4.35	4.56	3,6; I
Cha F34	K3 V:	0.79:	3.66:	5.1:	3,6,8; I,III
Cha F35	G3 V	0.02	—	—	2; I
Cha F36	K0 III	1.22	5.18	4.67	3,6; I
Cha F37	G9 III	0.32	1.09	3.75	1
Cha F38	A3 V	0.24	0.78	3.57	2; VI
Cha F39	K3 III	0.30	0.72	2.64	1
Cha F40	B8 III	0.65	1.95	3.30	1,2; III
Cha F41	B8 V	0.26	0.93	3.93	2; I,III
Cha F42	A3.5 IV	0.34	1.02	3.30	2; I,III
Cha F43	K5 III	0.25	0.78	3.43	2; I,III
Cha F44	A0 V	0.00	—	—	2,5; VI
Cha F45	F6 V	0.04	—	—	2; I
Cha F46	G2 V	0.05	—	—	2; I
Cha F47	A5 III–IV	0.04	—	—	2,5; VI
Cha F48	B9.5 V	0.18	0.50	3.1:	2; I,VI
Cha F49	F2 V	0.11	—	—	2; I
Cha F50	A8 IV	0.14	0.43	3.4:	2; I,VI
Cha F51	F7 V	0.10	—	—	2,5; VI
Cha F52	B9.5 V	0.30	0.90	3.30	2; I,III
Cha F53	F6 V	0.04	0.14	—	2; I,III
Cha F54	G6 III–IV	0.28	0.87	3.42	2,5; III,VI
Cha T21	G2-5 V	0.72	3.30	5.04	3,4,9,10,11; I,IV
Cha T41	B9 V	0.43	1.97	5.04	2,6,9,12,13; I,II

sample, with ranges coded by plotting symbol. The two distributions are consistent, with a clear tendency in each case for the highest values ($\lambda_{max} > 0.65\,\mu$m; $R_V > 4.5$) to occur in the central and southern regions of the field bounded by coordinates RA $11^h\,00^m$ to $11^h\,10^m$ and Dec. $-77°40'$ to $-76°00'$. This region of the cloud contains the highest density of in-

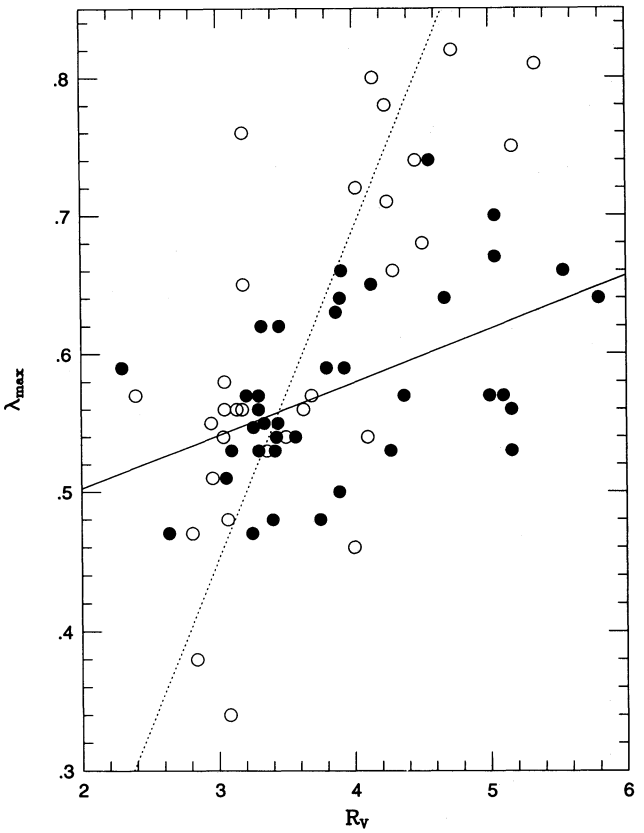

Figure 4. Plot of λ_{max} versus R_V for 38 Cha I stars (filled circles) compared with 30 stars from Clayton & Mathis (CM, open circles). The solid and dashed lines are linear least squares fits to the Cha I and CM data, respectively. The fits are $\lambda_{max} = 0.038R_V + 0.43$ (solid line) and $\lambda_{max} = 0.24R_V - 0.27$ (dashed line).

terstellar matter (as indicated by $C^{18}O$ contours in Fig. 5) and concentrations of recent star formation centred on the reflection nebulae Ced 110, 111 and 112 and their illuminating stars (Paper II; Paper IV). Our data support the conclusions of Vrba & Rydgren (1984): values of R_V and λ_{max} tend to be 'normal' (close to 3.1 and 0.55 μm, respectively) in the outer parts of the cloud, but exhibit significant increases towards the dense core. This is consistent with a general scenario in which grain growth via coagulation or mantle growth proceeds with greatest efficiency in the densest regions of the cloud (Whittet 1992). Clearly, both λ_{max} and R_V measure grain properties that respond similarly to environment, even though they do not correlate closely with each other (Section 3.2 above).

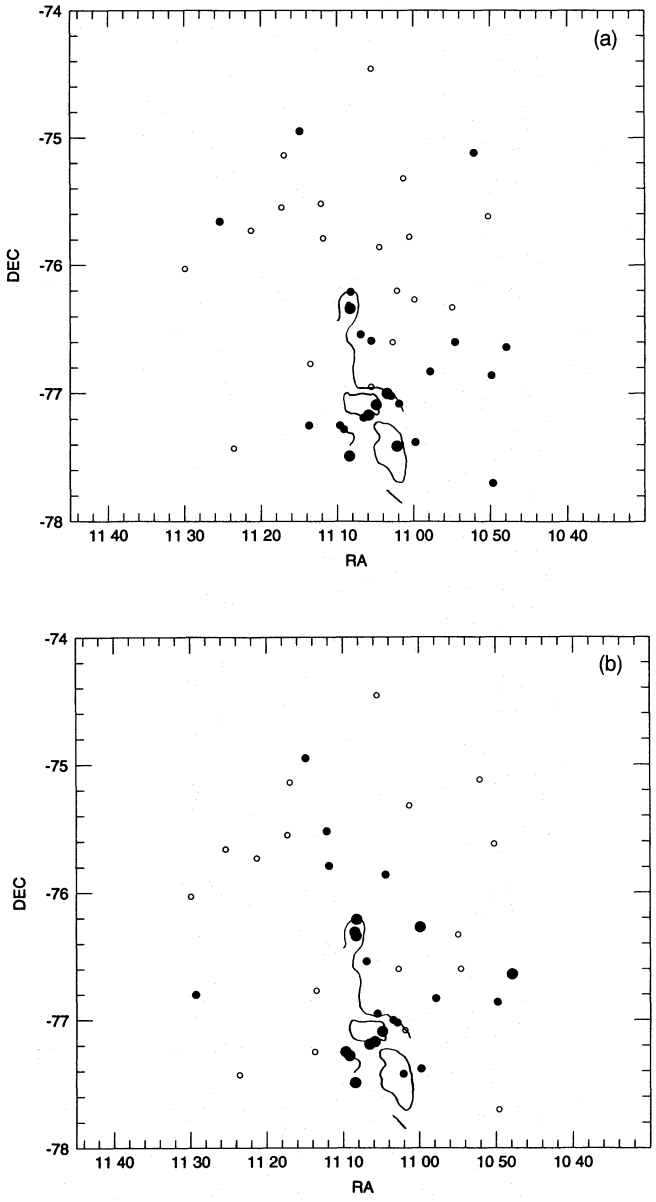

Figure 5. Spatial distributions of (a) λ_{max} and (b) R_V. Regions of highest density in the cloud are indicated by $C^{18}O$ contours from Mattila, Liljeström & Toriseva (1989). The symbols denote the range of each parameter: (a) open circles: $\lambda_{max} \leq 0.55\,\mu$m; small solid circles: $0.55\,\mu\text{m} < \lambda_{max} < 0.65\,\mu$m; large solid circles: $\lambda_{max} \geq 0.65\,\mu$m; (b) open circles: $R_V \leq 3.5$; small solid circles: $3.5 < R_V < 4.5$; large solid circles: $R_V \geq 4.5$.

4 MAGNETIC FIELD AND GRAIN ALIGNMENT

4.1 Alignment efficiency

The ratio of polarization to extinction or reddening provides a measure of the efficiency with which the grains are aligned. However, it is also influenced by a number of other factors, including the homogeneity of the magnetic field, the number of clouds in the line of sight, and their structure, and the viewing angle with respect to the average magnetic field direction (e.g. Whittet 1992). Correlation studies involving large numbers of stars show the existence of an upper bound in the p versus E_{B-V} diagram, given according to Serkowski et al. (1975) by

$$p_{max}/E_{B-V} = 9 \text{ per cent mag}^{-1}. \quad (4)$$

Equation (4) represents optimum alignment in the Serkowski et al. sample, the various effects noted above tending to *reduce* the p/E_{B-V} ratio from this optimum value. Fig. 6(a) shows the correlation between p_{max} and E_{B-V} for Cha I, based on data from Tables 4, 5 and 6: the sample contains 38 stars and is identical to that used to investigate the λ_{max}–R_V correlation in Section 3.2 (Fig. 4) above. Fig. 6(a) also shows the straight line defined by equation (4). It is evident from this comparison that there are many stars with p_{max}/E_{B-V} values well above this nominal upper limit, suggesting that the degree of alignment efficiency is exceptional in Cha I. However, the total extinction A_V is a truer measure of the column density of dust than the reddening E_{B-V}, and the two parameters are not

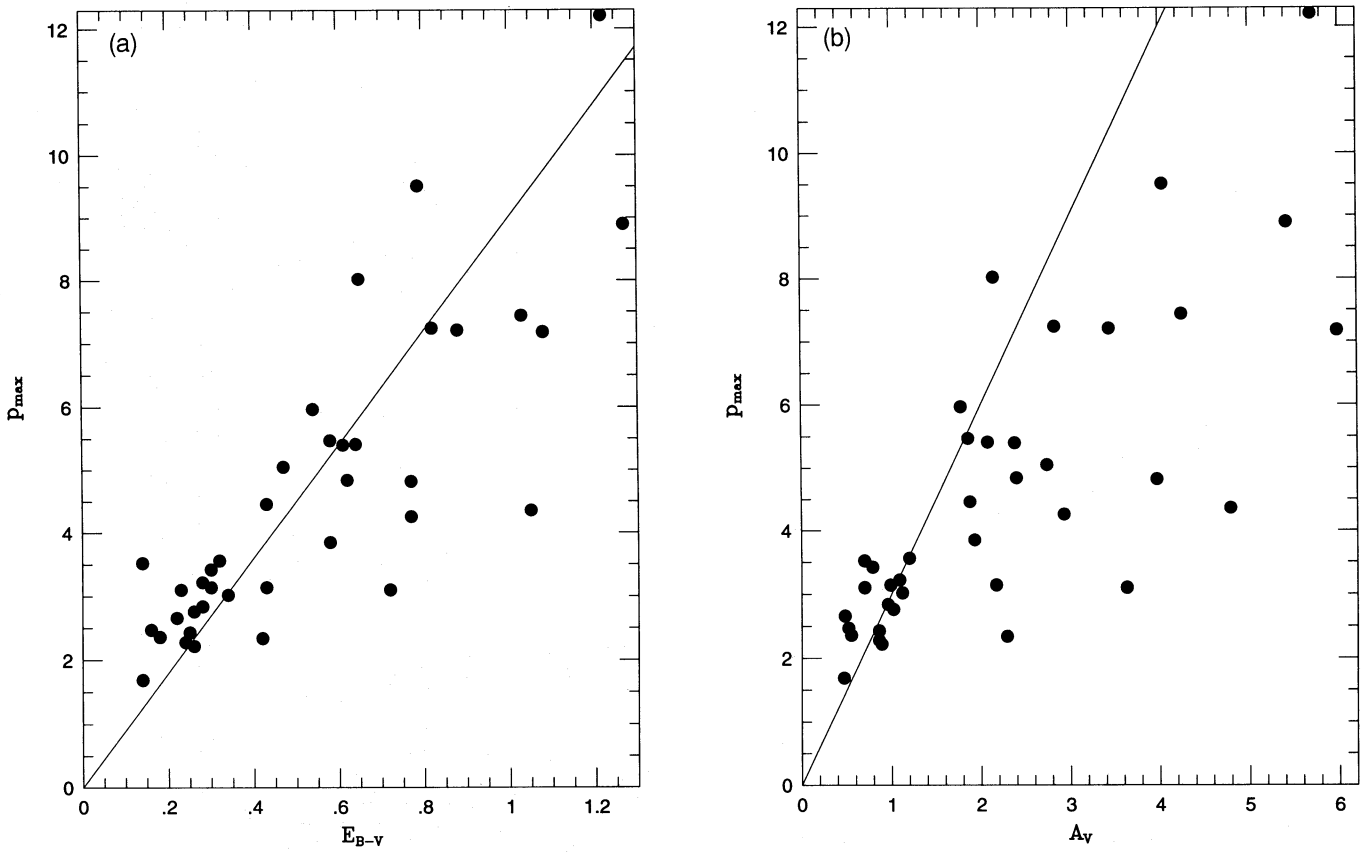

Figure 6. Plots of polarization (p_{max}) against (a) reddening (E_{B-V}) and (b) extinction (A_V). In each case, the straight line represents optimum alignment in the general interstellar medium (equation 4) according to Serkowski et al. (1975), assuming $A_V = 3E_{B-V}$ in case (b).

directly equivalent because of the variability demonstrated in R_V. We plot p_{max} against A_V in Fig. 6(b). The straight line is $p_{max}/A_V = 3$ per cent mag^{-1}, which is equivalent to equation (4) when $R_V = 3$, as appropriate for the Serkowski et al. sample in which the majority of stars are subject to diffuse-cloud extinction. There are notably fewer stars lying to the left of the line in Fig. 6(b) compared with Fig. 6(a), supporting the view that A_V is, indeed, the correct parameter to use in this context. The degree of alignment, as measured by p_{max}/A_V, is nevertheless exceptionally high in several lines of sight in Cha I compared with more typical regions of the interstellar medium: a reasonable upper bound to the Cha I data would be $p_{max}/A_V \simeq 4.5$ per cent mag^{-1}. This result suggests that depolarization effects are unimportant and that our line of sight to Cha I is essentially perpendicular to uniform magnetic field lines.

There is some evidence in Fig. 6(b) to suggest that alignment is systematically less efficient towards stars with higher extinctions. This effect can be seen more clearly in Fig. 7, which plots alignment efficiency (p_{max}/A_V) against extinction (A_V). Although there is considerable scatter, a clear trend of decreasing alignment efficiency with increasing extinction is apparent. Tamura et al. (1987) found a similar dependence in Heiles Cloud 2 within the Taurus dark cloud complex. If one argues that the lines of sight with highest extinction tend to sample the densest regions of dark clouds, then the results suggest that the alignment mechanism becomes systematically less effective with increasing density.

A plausible scenario that might simultaneously explain the trend in Fig. 7 and the rather poor correlation between λ_{max} and R_V for the Cha I sample in Fig. 4 is one in which the polarization is produced preferentially in the outer layers of the cloud, where both λ_{max} and R_V are close to their normal interstellar values. In lines of sight that penetrate deeper into the cloud, R_V is increased by grain growth, but λ_{max} will be less affected if those grains responsible for high R_V are either more closely spherical or less efficiently aligned than the grains in the outer layers of the cloud. The extinction is then dominated by grains in the dense regions, the polarization by grains in the diffuse outer layers. This scenario is in qualitative agreement with the suprathermal mechanism of grain alignment (Purcell 1979), in which grains acquire rotational energy as a result of H_2 formation on their surfaces. In the dense inner regions of the cloud, much of the hydrogen will already be in molecular form, and the mechanism is thus inherently less efficient than it is in the outer layers.

4.2 Field geometry

The standard interpretation of interstellar polarization is that the long axes of interstellar grains tend to be orientated perpendicular to the magnetic field. The distribution of polarization vectors on the sky thus provides a two-dimensional representation of the local magnetic field. Fig. 8 shows the distribution of infrared polarization vectors in the Cha I cloud, combining J-band data from this paper (Table 1) and Whittet

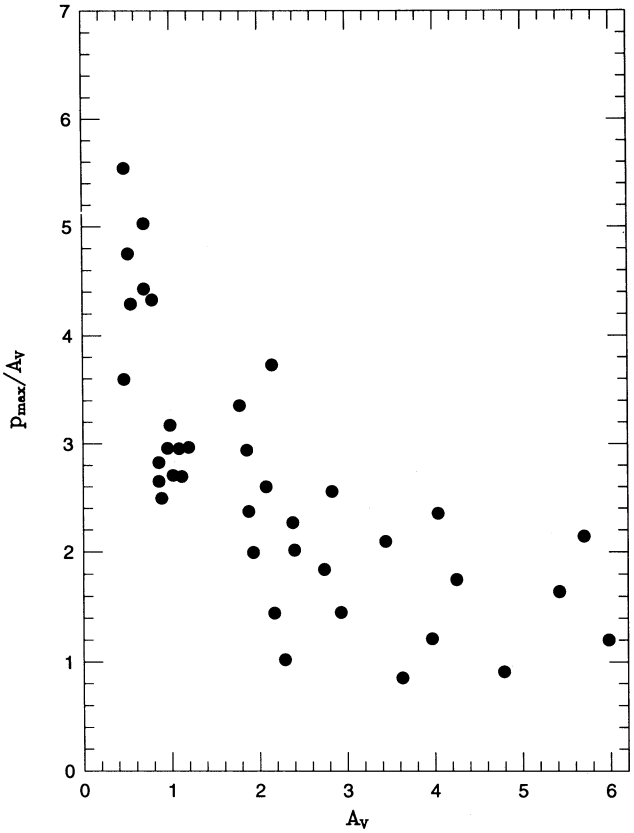

Figure 7. Plot of alignment efficiency (p_{max}/A_V) against visual extinction (A_V).

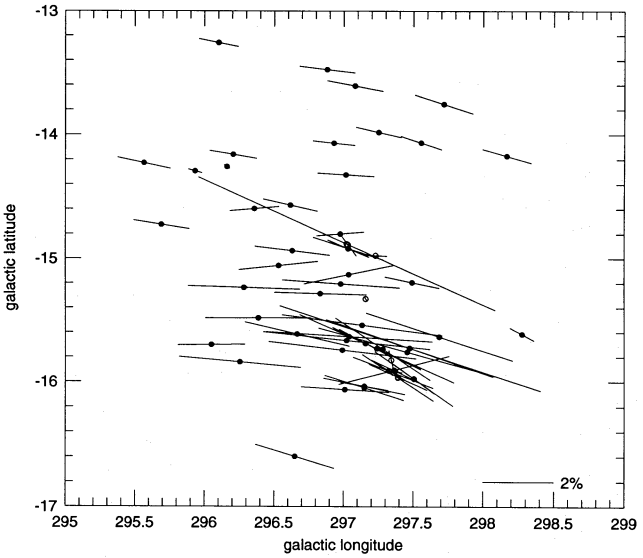

Figure 8. Map of polarization vectors in Cha I. Solid circles: *J*-band data from this paper (Table 1) and Whittet et al. (1992); open circles: *H* band from McGregor et al. (1994).

et al. (1992), and *H*-band data from McGregor et al. (1994). The lack of rotation in position angle for virtually all stars in Cha I with good spectral coverage justifies using measurements in two passbands to increase the data set. There is considerable uniformity in the plot, consistent with the high alignment efficiency noted above and the implied lack of depolarization effects which can result from a complex field geometry. The

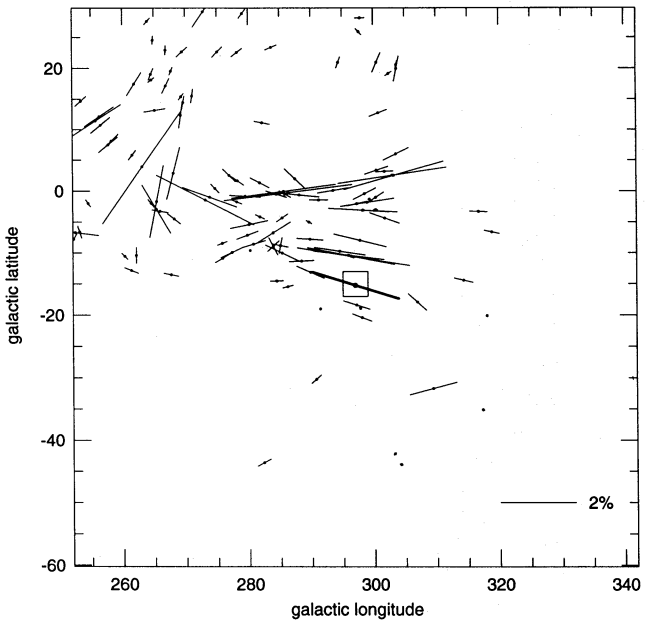

Figure 9. Map of visual polarization vectors in the Galactic neighbourhood around Cha I. The box corresponds to Fig. 8, with the thick line representing the average *J*-band polarization vector for the cloud.

general trend of the field is in a direction roughly perpendicular to the long axis of the cloud, as previously noted by McGregor et al. (1994). The shape of the cloud is thus consistent with collapse preferentially along magnetic field lines, with magnetic pressure continuing to support the cloud in its long dimension.

Goodman et al. (1990) noted that, in a number of dense clouds studied with optical polarimetry, the orientation of the field towards the cloud is very close to the macroscopic field orientation external to the cloud. We have examined this possibility for Cha I, using data from Mathewson & Ford (1970) and Axon & Ellis (1976) to construct a map of visual polarization vectors in the Galactic neighbourhood of Chamaeleon. The result is shown in Fig. 9. The box centred at $\ell = 297\overset{\circ}{.}0$, $b = -15\overset{\circ}{.}2$ corresponds to the area of sky in Fig. 8, containing the cloud, and the mean infrared (*J* band) polarization in Cha I is plotted as a thick bar centred on the box. Fig. 9 illustrates that there is general agreement in field direction, comparing Cha I with stars within 10°–15° of the cloud centre, suggesting that the cloud condensed uniformly from the local interstellar medium.

5 CONCLUSIONS

The main conclusions to emerge from this study are as follows.

(1) The wavelength dependence of polarization in Cha I is well represented by the Serkowski empirical formula with λ_{max} values in the range 0.47 to 0.75 μm. The correlation of the width parameter K with λ_{max} is similar to that found in other regions (Whittet et al. 1992).

(2) The correlation of λ_{max} with R_V is surprisingly poor. The most probable interpretation of this result is that not all the grains responsible for extinction in the blue-visible region (which effectively determines R_V; see Clayton & Mathis 1988) are aligned to the same degree: there may be spatial separation

of highly aligned grains (which dominate the polarization) and modified grains (which produce high R_V).

(3) The ratio of polarization to extinction is remarkably high in Cha I, with $p_{max}/A_V \simeq 4.5$ per cent mag^{-1} in some lines of sight. This may not be explicable purely in terms of fortuitous circumstances such as favourable viewing geometry and simple cloud structure, but may require a degree of local enhancement in either the magnetic field strength or the properties of the grains themselves that lead to alignment, such as their magnetic susceptibility.

(4) The decline in alignment efficiency with increasing extinction (Fig. 7) suggests that suprathermal spin-up may play some part in aligning the grains in the outer layers of the cloud. Our data for Cha I will provide important constraints on future studies of the grain alignment mechanism.

(5) The average direction of the magnetic field towards the cloud, projected in the plane of the sky, is perpendicular to the long axis of the cloud and parallel to the magnetic field in the Galactic neighbourhood of Chamaeleon, suggesting that the cloud formed by uniform collapse along magnetic field lines.

ACKNOWLEDGMENTS

We are grateful to the Panel for the Allocation of Telescope Time for an award of observing time on the Anglo-Australian Telescope, and to the Science & Engineering Research Council (UK) and the Natural Sciences & Engineering Research Council of Canada for financial support. This research has made use of the Simbad data base, operated at CDS, Strasbourg, France. We also thank Peter McGregor for a preprint.

REFERENCES

Assendorp R., Wesselius P.R., Whittet D.C.B., Prusti T., 1990, MNRAS, 247, 624 (Paper II)
Axon D.J., Ellis R.S., 1976, MNRAS, 177, 499
Bessell M.S., 1979, PASP, 91, 589
Bessell M.S., Brett J.M., 1988, PASP, 100, 1134
Blanco V.M., Demers S., Douglass G.G., FitzGerald M.P., 1968, Publ. US Naval Obs., Vol. 21
Bouchet P., Manfroid J., Schmider F.X., 1991, A&AS, 91, 409
Brindle C., Hough J.H., Bailey J.A., Axon D.J., Hyland A.R., 1986, MNRAS, 221, 739
Clarke D., Stewart B.G., 1986, Vistas Astron., 29, 27
Clayton G.C., Mathis J.S., 1988, ApJ, 327, 911 (CM)
Feigelson E.D., Kriss G.A., 1989, ApJ, 338, 262
Feigelson E.D., Casanova S., Montmerle T., Guibert J., 1993, ApJ, 416, 623
Glass I.S., 1979, MNRAS, 187, 305
Goodman A.A., Bastien P., Myers P.C., Ménard F., 1990, ApJ, 359, 363
Grasdalen G., Joyce R., Knacke R.F., Strom S.E., Strom K.M., 1975, AJ, 80, 117
Gregorio-Hetem J., Lépine J.R.D., Quast G.R., Torres C.A.O., de la Reza R., 1992, AJ, 103, 549
Grinin V.P., Kiselev N.N., Minikulov N.K., Chernova G.P., Voshchinnikov N.V., 1991, Ap&SS, 186, 283
Houk N., Cowley A.P., 1975, University of Michigan catalogue of spectral types, Vol. 1. University of Michigan, Ann Arbor
Hyland A.R., Jones T.J., Mitchell R.M., 1982, MNRAS, 201, 1095
Johnson H.L., 1966, ARA&A, 4, 193
Jones T.J., Hyland A.R., Harvey P.M., Wilking B.A., Joy M., 1985, AJ, 90, 1191
Kilkenny D., Whittet D.C.B., Davies J.K., Evans A., Bode M.F., Robson E.I., Banfield R.M., 1985, S. Afr. Astron. Obs., Circ., 9, 55
King D.J., 1981, PhD thesis, University of New South Wales
McGregor P.J., Harrison T.E., Hough J.H., Bailey J.A., 1994, MNRAS, 267, 755
Mathewson D.S., Ford V.L., 1970, Mem. R. Astron. Soc., 74, 139
Mathis J.S., 1986, ApJ, 308, 281
Mattila K., Liljeström T., Toriseva M., 1989, in Reipurth B., ed., Low mass star formation and pre-main-sequence objects. ESO Conf. Proc. No. 33, p. 153
Menzies J.W., Banfield R.M., Laing J.D., 1980, S. Afr. Astron. Obs., Circ., 5, 149
Menzies J.W., Cousins A.W.J., Banfield R.M., Laing J.D., 1989, S. Afr. Astron. Obs., Circ., 13, 1
Mouschovias T. Ch., Morton S.A., 1991, ApJ, 371, 296
Prusti T., Clark F.O., Whittet D.C.B., Laureijs R.J., Zhang C.Y., 1991a, MNRAS, 251, 303 (Paper IV)
Prusti T., Whittet D.C.B., Wesselius P.R., 1991b, Mem. Soc. Astron. It., 62, 775
Prusti T., Whittet D.C.B., Wesselius P.R., 1992, MNRAS, 254, 361 (Paper V)
Purcell E.M., 1979, ApJ, 231, 404
Rydgren A.E., 1980, AJ, 85, 444
Schmidt-Kaler Th., 1982, in Landolt-Börnstein New Series, Vol. 2b
Schwartz R.D., 1991, in Reipurth B., ed., Low mass star formation in southern molecular clouds. ESO Scientific Report No. 11, p. 93
Serkowski K., Mathewson D.S., Ford V.L., 1975, ApJ, 196, 261
Tamura M., Nagata T., Sato S., Tanaka M., 1987, MNRAS, 224, 413
Vrba F.J., Rydgren A.E., 1984, ApJ, 283, 123
Wardle J.F.C., Kronberg P.P., 1974, ApJ, 194, 249
Waters L.B.F.M., Coté J., Aumann H.H., 1987, A&A, 172, 225
Whittet D.C.B., 1992, Dust in the galactic environment. Institute of Physics Publishing, Bristol
Whittet D.C.B., van Breda I.G., 1978, A&A, 66, 57
Whittet D.C.B., van Breda I.G., 1980, MNRAS, 192, 467
Whittet D.C.B., Kirrane T.M., Kilkenny D., Oates A.P., Watson F.G., King D.J., 1987, MNRAS, 224, 497 (Paper I)
Whittet D.C.B., Prusti T., Wesselius P.R., 1991, MNRAS, 249, 319 (Paper III)
Whittet D.C.B., Martin P.G., Hough J.H., Rouse M.F., Bailey J.A., Axon D.J., 1992, ApJ, 386, 562
Wilking B.A., Lebofsky M.J., Martin P.G., Rieke G.H., Kemp J.C., 1980, ApJ, 235, 905
Wilking B.A., Lebofsky M.J., Rieke G.H., 1982, AJ, 87, 695

APPENDIX A: THE MEMBERSHIP STATUS OF F29 AND F34

Since the original compilation of field stars presented in Paper I, new data have indicated that two objects originally classified as field stars, F29 and F34, are actually probable members of the T-association. Optical spectra of F29 and F34 by Feigelson & Kriss (1989) and Gregorio-Hetem et al. (1992), respectively, suggest that both are weak-lined T Tauri stars. This interpretation is supported by the fact that both stars are X-ray sources (F29 = CHX 10 = CHXR 28; F34 = CHXR 47; Feigelson & Kriss 1989; Feigelson et al. 1993). As potential members, they may have an additional component to their polarized light due to scattering in surrounding circumstellar material (see discussion in Grinin et al. 1991). However, the spectral dependances of polarization in both objects follow the expected functional form (equation 1) for interstellar polarization, suggesting that interstellar polarization dominates over any intrinsic component. This conclusion is supported by the lack of significant near-infrared excess emission (Fig. 3). Inclusion of these stars in our analysis of the interstellar polarization properties of the Cha I cloud is therefore justified.

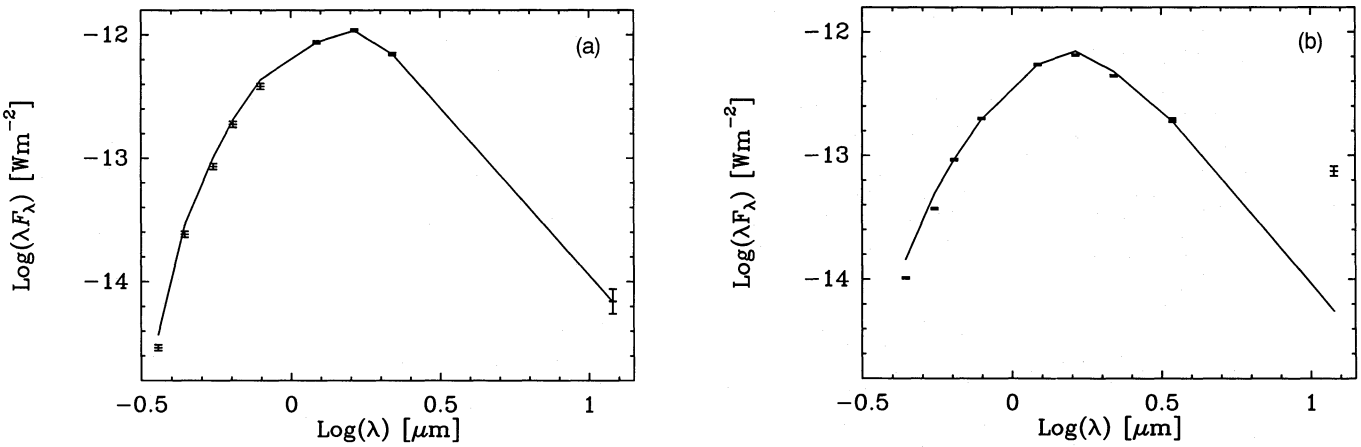

Figure A1. The observed spectral energy distributions of (a) F29 and (b) F34, compared with models described in Appendix A.

On the assumption that their polarizations are, indeed, primarily interstellar, the results of this paper lend support to the assignment of dwarf rather than giant intrinsic colours to F29 and F34, consistent with membership status. If (as in Paper I) we assign intrinsic colours appropriate to background field giants, the resulting colour excesses ($E_{B-V} = 0.31$ for F29, $E_{B-V} = 0.53$ for F34) are anomalously low in comparison to the degree of polarization. With dwarf intrinsic colours (Table 6), both stars occupy normal positions in the p versus E_{B-V} diagram (Fig. 6(a)), whereas giant intrinsic colours would place them well to the left of the general trend.

As an independent check on their status, we have attempted to model the observed spectral energy distributions of F29 and F34 (Fig. A1) by fitting them with simple models based on standard intrinsic colours. Intrinsic colours were taken from Bessell (1979), Bessell & Brett (1988) and Waters, Coté & Aumann (1987) for optical, near-infrared and *IRAS* data respectively, and these were corrected for interstellar extinction assuming values of E_{B-V} and R_V from Table 6. The models are normalized to the observations in the J passband (1.25 μm).

For F29, the spectral type (K7) is from Feigelson & Kriss (1989), and on the basis of the above discussion we assign luminosity class V. Optical and near-infrared photometry is from Paper I, and the 12-μm *IRAS* flux is from Prusti, Whittet & Wesselius (1991b). The fit to F29 (Fig. A1(a)) is within observational errors at all relevant wavelengths. Although the spectral energy distribution of F29 can be explained without evoking infrared excess, we nevertheless deduce this star to be a pre-main-sequence object. This conclusion is based on the absolute magnitude of a K7 V star (Schmidt-Kaler 1982) which would place F29 at a distance of 30 pc, too close for a reddened object in the Chamaeleon field where significant extinction sets in only at 140 pc (Paper I). We therefore conclude that F29 is a member of Cha I with excess luminosity consistent with its pre-main-sequence nature.

The spectral type (K3) of F34 is from Paper I, and again we assign luminosity class V. Optical and infrared photometry is from Papers I and III, respectively. The fit to F34 (Fig. A1(b)) shows that the far-infrared excess discussed in Paper III sets in at wavelengths longward of 3.5 μm. Like F29, F34 must have excess luminosity consistent with a pre-main-sequence phase of evolution: the absolute magnitude of a K3 V star (Schmidt-Kaler 1982) would place F34 at a distance of only 42 pc.

This paper has been produced using the Blackwell Scientific Publications TEX macros.